

RESEARCH ARTICLE

High-grade bladder cancer cells secrete extracellular vesicles containing miRNA-146a-5p and promotes angiogenesis

Marta Prieto-Vila¹ | Wataru Usuba² | Yusuke Yoshioka¹ | Fumitaka Takeshita³ | Miki Yoshiike² | Hideo Sasaki² | Yusuke Yamamoto⁴ | Eiji Kikuchi² | Takahiro Ochiya¹ 

¹Department of Molecular and Cellular Medicine, Institute of Medical Science, Tokyo Medical University, Tokyo, Japan

²Department of Urology, St. Marianna University School of Medicine, Kawasaki, Japan

³Division of Fundamental Innovated Oncology, National Cancer Center Research Institutes, Tokyo, Japan

⁴Laboratory of Integrative Oncology, National Cancer Center Research Institute, Tokyo, Japan

Correspondence

Takahiro Ochiya, Tokyo Medical University, 6-7-1 Nishi-Shinjuku, Shinjuku-ku, Tokyo 160-0023, Japan.
Email: tochiya@tokyo-med.ac.jp

Marta Prieto-Vila and Wataru Usuba contributed equally to this work.

Funding information

Japan Society for the Promotion of Science, Grant/Award Number: Grant-in-Aid for Young Scientists JSPS KAKENHI Gra; Japan Agency for Medical Research and Development, Grant/Award Number: Development of Diagnostic Technology for Detection

Abstract

Recurrence is one of the major issues in bladder cancer (BCa). Novel technologies, such as the detection of microRNAs carried by extracellular vesicles (EVs) in urine, have been proposed as biomarkers for detecting recurrence in BCa. Although the usefulness of microRNAs in body fluids from cancer patients has been reported, it is also known that they play essential roles in cancer progression. We previously proposed miR-146a-5p as a prognostic marker in BCa, since its urinary expression was associated with grade and tumour depth. However, the specific mechanisms of miR-146a-5p remain unclear. Here, we show the proangiogenic effects of miR-146a-5p secreted by high-grade BCa cells. The urinary miR-146a-5p level was higher in patients with high-grade BCa than in those with low-grade BCa. Similarly, tumours generated by miR-146a-overexpressing BCa cells in mice grew rapidly with high levels of angiogenesis. BCa-derived EV treatment promoted the proliferation of endothelial cells via the inhibition of the demethylase TET2 and the subsequent increase in its downstream target c-Myc. These findings demonstrate that secreted miR-146a-5p contributes to cancer progression by promoting angiogenesis. Therefore, miRNAs in EVs may become not only a diagnostic tool but also a target molecule for therapy.

KEYWORDS

angiogenesis, bladder cancer, cancer, EVs, microRNA

1 | INTRODUCTION

Bladder cancer (BCa) is the most common urinary cancer (Sung et al., 2021). There were approximately 570,000 new cases of BCa and 210,000 related deaths in 2020 (Sung et al., 2021). Other cancers, such as breast or prostate cancer, have powerful diagnostic methods, such as PSA detection (Sadi, 2017), which have improved the outcome of patients by early detection (Ulmert et al., 2008). However, this is not the case with BCa, which has not yet a specific tumour marker (Oude Elferink & Witjes, 2014; Stănescu et al., 2014). Basic methods for the diagnosis and surveillance of BCa include cystoscopy, urine cytology, and ultrasound sonography. However, those classical methods are a two-sided coin. For instance, cystoscopy has high precision but high invasiveness, and urine cytology has the opposite characteristics. Notably, one of the most terrible abilities of BCa is its high recurrence rate. Patients with non-muscle invasive BCa experience 5-year recurrence-free survival rates of 23 to 43% (Lenis et al., 2020). Recurrence is especially important in the case of high-grade cancer, which is more aggressive and possesses high invasive ability, translating

This is an open access article under the terms of the [Creative Commons Attribution-NonCommercial-NoDerivs License](https://creativecommons.org/licenses/by-nc-nd/4.0/), which permits use and distribution in any medium, provided the original work is properly cited, the use is non-commercial and no modifications or adaptations are made.

© 2022 The Authors. *Journal of Extracellular Biology* published by Wiley Periodicals, LLC on behalf of the International Society for Extracellular Vesicles.

to a worse prognosis (Damrauer et al., 2014). Therefore, sensitive and non-invasive methods for BCa are strongly needed for recurrent medical examinations.

MicroRNAs (miRNAs) are noncoding RNAs composed of 18–24 base pairs with single-chain molecules (Bartel, 2004; Xiu et al., 2014). Their biological role is to act as RNA interference molecules; they prevent the protein output of their target genes by binding to a specific 3′-untranslated region of the mRNA strand (Carthew & Sontheimer, 2009). They are present in all cells and can be secreted into the extracellular space. Therefore, they can be found in most, if not all, biological fluids, including urine. Since miRNAs regulate multiple functions, their expression is altered in cancer (Carlos & Slack, 2006; Zhang et al., 2007). Hence, cancer-specific altered expression can be detected and used as a diagnostic marker.

miRNA is known to be packaged within extracellular vesicles (EVs). EVs are lipid bilayer nanoparticles secreted from cells that contain multiple nucleic acids, such as DNA, mRNA, and miRNA, as well as proteins. EVs transport cargo into receptor cells and are essential intercellular communication tools. As mentioned, the lipid bilayer of EVs confers protection of molecules outside the cell, such as miRNA, that would degrade shortly otherwise. For these reasons, miRNAs encapsulated in EVs have attracted considerable attention for their use as biomarkers in cancer (Gould & Raposo, 2013).

In addition to the possible use of EV-encapsulated miRNA as a diagnostic tool, these same miRNAs play many essential roles in cancer as microenvironment modulators, which in turn favours cancer cell growth and metastasis (Peinado et al., 2012; Skog et al., 2008; Yokoi et al., 2017). EVs also promote endothelial cell (EC) growth, inducing tumour angiogenesis (Deregibus et al., 2007). Angiogenesis is a vital process for the development of tumours since it supplies cancer cells with the nutrients and oxygen necessary for their growth (Carmeliet, 2000). Furthermore, the newly formed tubes also provide a route for metastatic cells to escape (Nishida et al., 2006).

MiR-146a-5p is a promising BCa biomarker. We previously reported that urinary miR-146a-5p was increased in patients with BCa and that this expression was reduced after treatment (Sasaki et al., 2016). However, the concrete role of miR-146a-5p in high-grade BCa has not been described. Understanding the mechanisms of cancer progression will help us to develop novel therapies. Since we reported that miR-146a-5p expression was high in bladder cancer patients, we hypothesized that its role could be important for cancer development. Here, we described a novel role of miR-146a-5p as an angiogenesis promoter, supporting tumour growth in high-grade BCa by the direct inhibition of the demethylase TET2 and the subsequent increase in c-Myc in EC.

2 | MATERIALS AND METHODS

2.1 | Clinical samples

Voided urine samples were obtained from 65 bladder cancer patients and 54 healthy controls. All samples were collected between 2016 and 2018 (Table S1). The urine samples were gently mixed with a pipette, and an aliquot of each sample was stored at -80°C . For formalin-fixed paraffin embedding (FFPE) samples, the samples were obtained from transurethral resection (TUR) of tumours and radical cystectomy. Twenty-one TUR and one cystectomy procedures were performed, and the specimens were stored between 2014 and 2016 (Table S2).

All human samples were collected under a study protocol approved by the institutional review board at St. Marianna University, and all subjects provided written informed consent.

2.2 | Cell culture

The human bladder cancer cell lines RT4, SW780, 5637, HT1170, HT1376, T24, UMUC-3, TCCSUP, and J82 and the human normal urothelial cell line SV-HUC-1 were obtained from the American Type Culture Collection (Manassas, VA, USA). All the cell lines were cultured with 10% heat-inactivated foetal bovine serum (Invitrogen, Carlsbad, CA, USA) and 1% antibiotic-antimycotic (Invitrogen). However, the basic medium was different depending on the cell type. HT1170, HT1376, T24, UM-UC-3, and J82 cells were cultured in Minimum Essential Medium Eagle's modified (Sigma–Aldrich, St Louis, MO, USA); the 5637 cells were cultured in RPMI 1640 basic (Gibco, SF, USA); the T24 and RT4 cells were cultured in McCoy's 5A (Sigma–Aldrich); the SV-HUC-1 cells were cultured in F-12K medium (Gibco); and the TCCSUP cells were cultured in Modified Eagle's Medium (Sigma–Aldrich) also containing Pyruvate Sodium 20 nM (Gibco).

All the cell lines were incubated at 37°C in 5% CO_2 and passaged when confluency reached 80%.

2.3 | Establishment of miR-146a-overexpressing cell lines

J82 and UMUC3-luc cell lines were transfected with the plasmids pCMV-miR-146a and pBApo-CMV as a negative control) as previously described (Kosaka et al., 2010). Transfected cells were selected with 700–1000 $\mu\text{g}/\text{ml}$ gentamicin (Gibco).

2.4 | Laser-capture microdissection (LCM)

For laser capture microdissection, FFPE samples were sliced (6 μm) on the plate. After deparaffinization and rehydration, the samples were stained with 0.05% toluidine blue for 20 s, which specifically stains epithelial cells. The dissection of normal and malignant epithelial cells was performed immediately by using a Leica LMD6500/7000 according to the manufacturer's protocol (Leica Microsystems, Wetzlar, Germany).

2.5 | Exosome extraction

Once the cell confluence reached 70%, the cells were washed with PBS, and the culture medium was replaced with advanced DMEM (Thermo Fisher Scientific) for RT4, SW780, HT1376, HT1170, T24, UM-UC-3, J82, and TCCSUP cells; advanced DMEM/Ham's F-12 medium (Thermo Fisher Scientific) for SV-HUC-1 cells; or advanced RPMI-1640 medium (Thermo Fisher Scientific) for 5637 cells containing antibiotic-antimycotic and 2 mM L-glutamine. After incubation for 48 h, the conditioned medium was collected and centrifuged at 2000 g for 10 min at 4°C. To remove cellular debris, the supernatant was filtered through a 0.22- μm filter (Millipore, Burlington, MA, USA). The conditioned medium was then used for EV isolation. Samples were ultracentrifuged at 24 000 g for 70 min at 4°C and resuspended in PBS.

Urine samples were centrifuged at 10 000 g for 10 min to separate the supernatant from the sediment fractions, which probably contained cells. One millilitre of the supernatant was transferred and ultracentrifuged at 24 000 g for 35 min at 4°C. All samples were resuspended in 100 μl of PBS.

The protein concentration of the EV fraction was determined using a Quant-iT Protein Assay with a Qubit 2.0 Fluorometer (Invitrogen).

2.6 | Nanoparticle tracking system

To determine the size distribution of the EVs, nanoparticle tracking analysis was carried out using the NanoSight LM10-HS system (NanoSight). The results are presented as the average \pm SE of three independent experiments of the 60-s video.

2.7 | PKH-67-labelled EV uptake in HUVECs

Purified EVs derived from 5637, UMUC-3, J82 miR-146a nc, and J82 miR-146a o/e cells were labelled with a PKH67 green fluorescence labelling kit (Sigma-Aldrich). EVs were incubated with 2 mM PKH67 for 5 min and washed five times using a 100-kDa filter (Microcon YM-100, Millipore) to remove excess dye. PKH67-labelled EVs were used to assess EV uptake *in vitro*. Before the addition of labelled EVs to the recipient cell, the particle number was calculated using the NanoSight system, and the same amount of labelled EVs was added to HUVECs (10^8 particles). Twelve hours later, the amount of uptaken EV in HUVECs was captured by confocal microscopy (Olympus, Tokyo, Japan).

2.8 | Cell proliferation assay (MTS assay)

For the cell proliferation assay, 48 h after transfection with miR-146a mimic (Guide chain: 5'-UGAGAACU-GAAUCCAUGGGUU-3', Passenger chain: 5'-CCUCUGAAAUUCAGUUCUUCAG-3') and the scramble negative control (Genedesign, Osaka, Japan) or EV addition, 5000 cells were seeded in a 96-well plate (Thermo Fisher Scientific). After 3 days of culture, the cell viability was measured by Cell Counting Kit-8 (Dojindo Molecular Technologies, Japan). Absorbance at 450 nm was read after 2 h of incubation at 37°C using a Synergy H4 Microplate Reader (BioTek, Winooski, VT, USA). Relative proliferation was calculated relative to untreated cells.

2.9 | RNA extraction and real-time quantitative PCR (RT-qPCR)

Total RNA from cultured cells and exosomal RNA was extracted using QIAzol and the miRNeasy Mini Kit (Qiagen, Hilden, Germany) according to the manufacturer's protocol. The extracted RNA concentration was measured by Nanodrop (Thermo Fisher Scientific). For FFPE samples, total RNA was extracted using a miRNeasy FFPE kit (Qiagen) according to the manufacturer's protocol.

The RNA was reverse transcribed with the TaqMan MicroRNA Reverse Transcription Kit (Applied Biosystems, Waltham, CA, USA) and the specific miRNA cDNA TaqMan probe. For mRNA expression analysis, 1 μg of total RNA was reverse transcribed with the High Capacity cDNA Reverse Transcription Kit (Applied Biosystems). The synthesized cDNAs were then quantified by

TaqMan Gene expression analysis on a StepOne Real-Time PCR System (Applied Biosciences). Relative fold changes in mRNA expression levels were calculated using the Formula $2^{-\Delta\Delta C_t}$ method. All reactions were performed in duplicate.

For tissue and cellular normalization, RNU48 (TaqMan assay ID: 001006) was used. Cel-miR-39 (TaqMan assay ID: 000200) was used in the EV fraction as an invariant factor in urine-derived samples and urine samples were normalized according to the particle number. For all miRNA assays, miR-146a-5p (TaqMan assay ID: 004068), as a target, was used in urine, tissue and cellular samples.

The β -actin (Taqman assay ID: Hs01060665) housekeeping gene was used to normalize the variation in mRNA samples. To confirm gene expression, TET2 (TaqMan assay ID: Hs00325999), ANKRD2 (TaqMan assay ID: Hs01074529), CYB5R4 (TaqMan assay ID: Hs01371146), ZNF667 (TaqMan assay ID: Hs00254426) and ZNF850 (TaqMan assay ID: Hs01371146) were used for qRT-PCR.

2.10 | Western blot

HUVECs treated with miR-146a mimic or EVs were lysed using Mammalian Protein Extract Reagent (Thermo Scientific, Rockford, IL, USA), and the protein concentration was measured using Qubit (Invitrogen). Total protein samples were separated using 4–15% gradient SDS-PAGE (MiniPROTEAN TGX Gel, GE Healthcare, IL, USA). After blocking with Blocking One (Nacalai Tesque, Japan) for 1 hr, primary antibodies were incubated overnight at 4°C. The primary antibodies used were TET2 (#MABE462, Millipore), c-Myc (#5605s, Cell Signaling Technologies, Danvers, MA, USA) and c-Actin (#MAB1501, Millipore). After three washes, the membranes were incubated for 1 h with an adequate secondary antibody linked to horseradish peroxidase anti-mouse IgG (#NA931, GE Healthcare, WI, USA) or anti-rabbit IgG (#NA934, GE Healthcare, WI, USA). Signals were developed using ImmunoStar LD (Wako, Japan). Images and consecutive quantification were performed using the Fusion solo software with a Fusion Solo S imaging system microscopy (Vilber, France).

2.11 | Microarray analysis

To detect the target gene of miR-146a-5p in HUVECs, cells were transfected with miR-146a mimic and the scramble negative control and treated with exosomes derived from 5637, T24, UMUC-3, J82 NC o/e and J82 miR-146a o/e cells. We compared the gene expression between the miR-146a o/e group and the negative control group.

The quantity and quality of the samples were calculated by a NanoDrop1000 spectrophotometer (Thermo Fisher Scientific) and Agilent Bioanalyzer (Agilent Technologies). One hundred nanograms of total RNA was amplified and labelled with a Low Input Quick Amp Labelling Kit (Agilent Technology) according to the manufacturer's protocol. Then, 0.60 μ g of Cy3 dye-labelled cRNA was hybridized onto a SurePrint G3 Human GE v2 8 \times 60K (Agilent Technologies; design ID: 072363). After scanning the microarray chip using an Agilent microarray DNA scanner (G4900DA), the intensity values were quantified using Agilent Feature Extraction software version 11.5.1.1. Normalization was performed using Agilent GeneSpring software version 14.9. Afterwards, genes with a change in signal ≥ 1.2 - or ≤ -1.2 -fold change were selected.

2.12 | Tube formation assay

A total of 10^4 HUVECs were cultured on 50 μ l of Matrigel (Sigma-Aldrich) in a reduced tube assay culture medium. The growth factors were reduced to 1/3 in comparison to the manufacturer's protocol. No other alterations were made. To evaluate the angiogenic potential of high-grade derived EVs, 10 μ g/ml EVs were added at the moment of cell transfection on the Matrigel. The degree of capillary tube formation was analysed after 16 h of culture and quantified by measuring all the branches and their lengths in each well ($n = 3$).

2.13 | Animal experiments

The animal experiments in this study were performed in compliance with the guidelines of the Institute for Laboratory Animal Research at the National Cancer Center Research Institute.

Six- to seven-week-old female C.B.17/SCID mice (Charles River Japan, Kanagawa, Japan) were anaesthetized, and 5×10^6 UMUC3-luc cells overexpressing miR-146a (miR-146a o/e) or empty vector were inserted through the urethra with a catheter after trypsin treatment of the bladder. This treatment allowed cancer cell retention on the bladder as an orthotropic model (Figure S2), referred to as the method for intravesical injection from Uchino K *et al.* (Uchino *et al.*, 2013). The development of subsequent tumour growth was monitored once a week by *in vivo* imaging. Mice were injected with 150 mg/kg D-luciferin

(Promega, Madison, WI, USA) intraperitoneally and imaged 10 min later to count the photons from the whole body using the IVIS imaging system (Xenogen, Alameda, CA, USA) according to the manufacturer's instructions. The data were analysed using LivingImage software (Xenogen). At 3 weeks after transplantation, the mice were sacrificed, and the tumours were resected and fixed in 4% paraformaldehyde phosphate buffer solution (Wako).

2.14 | Immunohistochemistry

Paraffin-embedded tissue samples from mouse experiments were rehydrated. Antigen unmasking was performed by heating the samples in Immunosaver (NEM, Japan) for 3 min at 120°C. After permeabilization, antigen retrieval, and blocking using Protein Block Serum-Free (Dako, Dinamarca), primary antibodies were used overnight at 4°C. The primary antibodies used were CD31 (#ab28364, Abcam, England) and HIF1 α (#NB100-105, Novus, St. Luis, MI, USA). Then, the samples were incubated for 1 h with ImPRESS IgG-peroxidase kits (Vector Laboratories, Burlingame, CA, USA). Finally, colour development was performed using an ImmPACT DAB substrate kit (Vector Laboratories) under light microscopy, followed by counterstaining with Mayer's haematoxylin (Applied Biosystems) for 3 min. The observation of the stained cells was performed by BZX-700 (KEYENCE, Osaka, Japan). Using CD31-positive cells, the area of blood vessels was calculated with BZ-H3M software (KEYENCE).

2.15 | 3'UTR assay

Plasmids containing the predicted wild-type and mutated target sequences of miR-146a-5p were generated as follows. A 481-bp fragment from the 3'UTR of TET2 (located at positions 2395–2402 of the TET2 3'UTR) was PCR-cloned from HUVECs. Three prime A-overhangs were added to the PCR products after 15 min of regular Taq polymerase treatment at 72°C. The PCR products were cloned into a pGEM-T easy vector (Promega). The amplified products were ligated into the NheI and Sall sites of the 3'UTR of the firefly luciferase gene in the pmirGLO Dual-Luciferase miRNA Target Expression vector (Promega) to generate pmiR-TET2. The primer sequences were as follows (shown 5' to 3'): TET2_F, GTGCTAGCATATATCACCCCCTTTTGTTGG and TET2_R, CAGTCGACTATTCCAGTATTTTCAGTACATC. Site-directed mutagenesis was performed in the seed sequences of TET2. PrimeStar Max DNA Polymerase (Takara, Kyoto, Japan) was used for PCR amplification. The forwards and reverse primer sequences were as follows (shown 5' to 3'): TET2_Mut_F, GTATCGGTATAATGACGTGGGCAGTGGGGA and TET2_Mut_R, TCATTATACCGATACTACTGACAGGTTGG.

For the 3'UTR assay, each vector plasmid combined with miRNA mimic transfection was performed with DharmaFECT Duo reagent (Horizon Discovery) in accordance with the manufacturer's protocol. Forty-eight hours after cotransfection with the 3'UTR assay vector (pmiR-TET2) and premiR-146a-5p, luciferase activity was measured using the Dual-Glo Luciferase Assay System (Promega) following the manufacturer's protocol. Firefly luciferase activity was normalized to *Renilla* luciferase activity.

2.16 | Kaplan Meier

Kaplan Meier Plots was draw using the online tool KM-plotter (Lánczky & Győrffy, 2021). We used all bladder cancer samples (404 patients) stratified by expression of TET2, C-MYC and a combination of both. The two cohorts' significance was calculated with a logrank *P* value with a 95% of interval confidence.

2.17 | Statistical analyses

More than four biological replicates were utilized in MTS assays. Fifteen biological replicates were used in mouse studies. All other studies utilized three biological replicates. All the data are presented as the mean \pm standard deviation. Statistical significance was calculated using a two-tailed Student's *t*-test or Bonferroni's test. Statistical significance was considered when the *P* value was < 0.05. * denotes *P* value < 0.05; **denotes *P* value < 0.01.

3 | RESULTS

3.1 | EV number and miRNA-146a-5p levels are high in high-grade BCa patients

In previous studies, we quantified the expression levels of miRNAs in urine from patients with BCa and healthy individuals and found higher levels of miR-146a-5p in BCa patients. Since this expression was analysed using the supernatant and sediment fractions combined and the sample number was quite small (24 samples), we repeated the measurement to include a total of 117 patients (Table S1). Moreover, we focused exclusively on exosomal miRNAs.

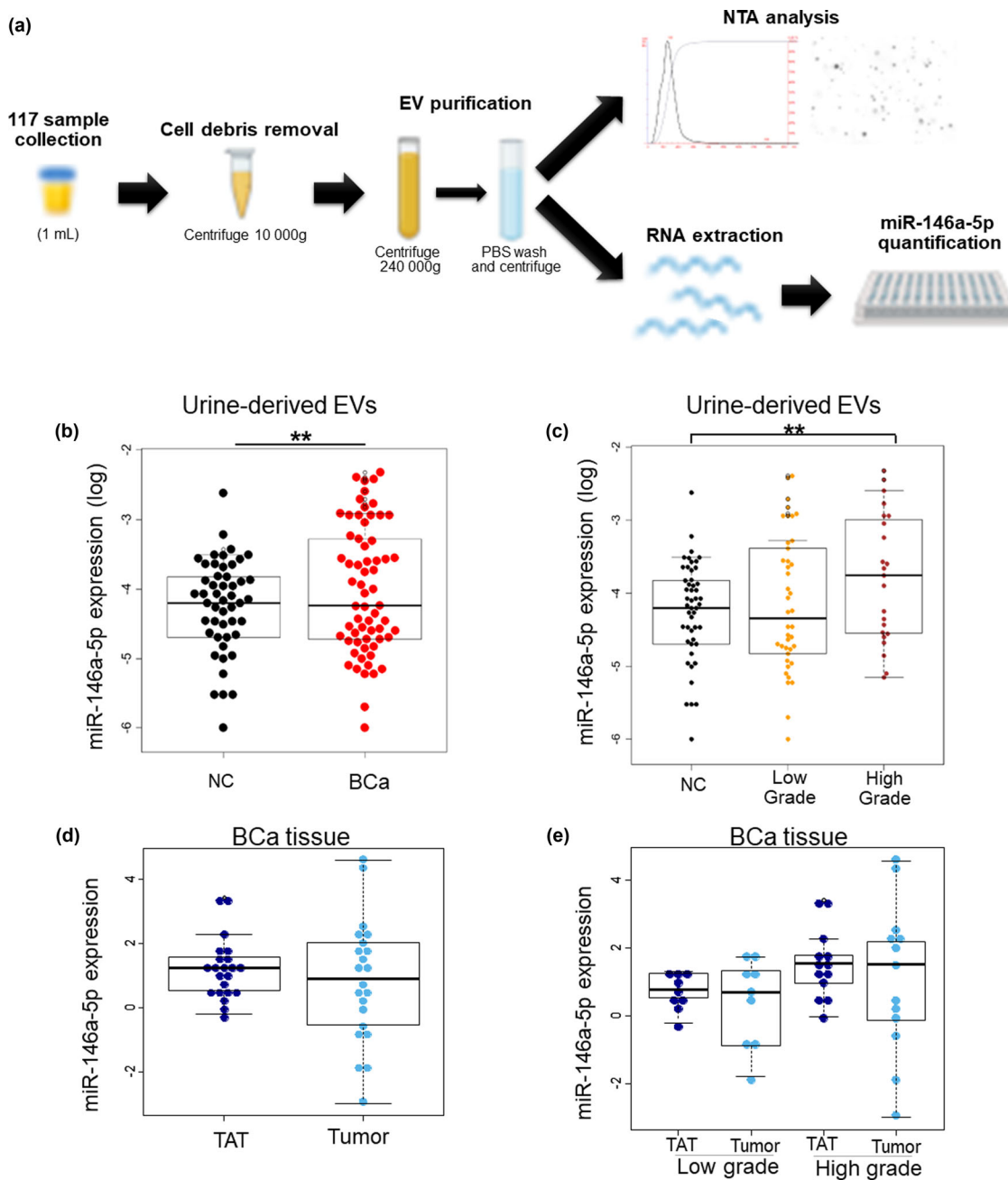


FIGURE 1 Urine levels of exosomal miR-146a-5p are increased in high-grade BCa patients. (a) Scheme of sample collection, EV isolation and further analyses. (b) Relative expression of exosomal miR-146a-5p to particle number in urine, separated by BCa and healthy individuals; $P = 0.005$. (c) Further separation according to the grade of BCa. NC versus high-grade $P = 0.008$. (d) Differential miR-146a-5p expression in tumour-adjacent tissue (TAT) and tissue cells. (e) Further separation according to the grade of BCa

To collect the EVs, a 1-ml urine sample was ultracentrifuged (Figure 1a). The particle number was analysed by Nanoparticle tracking analysis (NTA), finding significantly higher levels of particles in cancer patients than in healthy individuals (NC vs. Low-Grade BCa $P = 0.005$; NC vs. High-Grade BCa $P = 0.01$). However, no significant differences were found between low- and high-grade BCa patients (Figure 1a) ($P = 0.095$). Next, RNA was extracted from EVs, and their miRNA content was analysed. Urinary miR-146a-5p was highly expressed in patients with bladder cancer (Figure 1b). This difference was greater when BCa patients were separated according to their grade of cancer, being higher in high-grade BCa (Figure 1c). However, there was no difference between healthy individuals and low-grade patients. Furthermore, a very low correlation (Spearman's correlation: $R = 0.22$; P value = 0.019) was found between particle number and miR-146a-5p expression levels in the patients' urine (Figure 1b). These results suggested that urinary miR-146a-5p expression is specifically higher in patients with BCa, especially in high-grade BCa, independent of the secreted particle number.

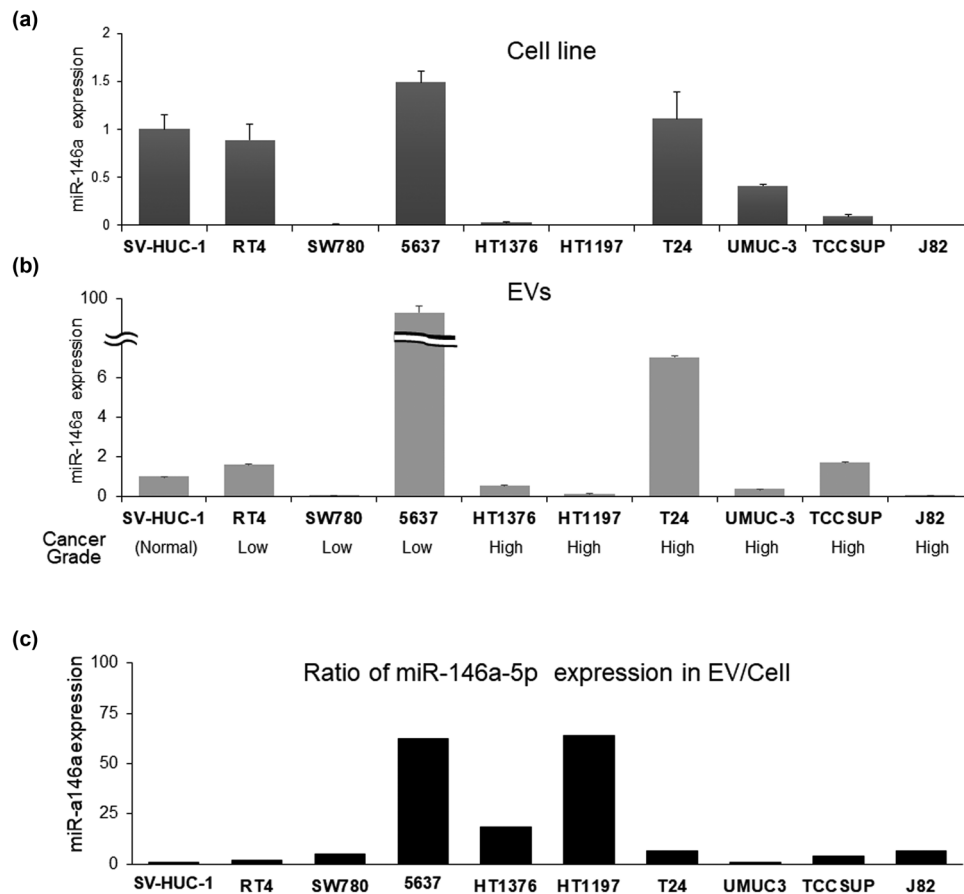


FIGURE 2 miR-146a is selectively enriched in EVs. (a) Relative expression of miR-146a-5p in several cell lines ($n = 3$). (b) Relative expression of miR-146a-5p in EVs derived from several BCa cell lines ($n = 3$). (c) Ratio between secreted miR-146a-5p and cellular expression, relative to the noncancerous cell line SV-HUC-1

Next, we investigated the origin of miR-146a-5p in clinical tissue samples by the comparison of the expression between tumour and tumour-adjacent tissue (TAT). The tissue of 22 samples (Table S2) was resected by laser-capture microdissection (LCM) (Figure S1c). When all the samples were analysed together, significant differences were not found (Figure 1d). Similarly, when samples were divided according to cancer grade, high-grade BCa expressed higher levels of miR-146a-5p (Figure 1e). Additionally, the expression of cellular miR-146a-5p, as well as secreted miR-146a-5p in EVs, was analysed in various BCa and normal urothelial cell lines (Figure 2a,b). EVs were confirmed by the expression of the typical EV markers CD9, and CD81, as well as the lack of expression of the endoplasmic reticulum marker, Calnexin (Figure S1d). Although most of the cell lines expressed miR-146a-5p levels similar to those of the noncancerous cell line SV-HUC-1, an apparent enrichment of miR-146a-5p levels secreted within EVs was observed in BCa cells, as shown by the ratio if secreted miR-146a versus the cellular expression (Figure 2c).

Since we found a significant difference between miR-146a-5p levels in urine between low- and high-grade BCa (Figure 1c), we next analysed the possible effects on the tumour microenvironment by analysing the tumour structure. Mean vessel density (MVD) was calculated by CD31 staining in samples ($n = 3$) of low- and high-grade BCa and showed a high difference in stained blood vessel area ($P < 0.04$). We observed that high-grade BCa patients released EVs containing miR-146-5p in urine, and those same patients showed a higher MVD, suggesting a role of miR-146a-5p in angiogenesis (Figure S1 e,f).

3.2 | Overexpression of miR-146a promoted tumour growth and angiogenesis in the orthotopic mouse model

Because we found a correlation between BCa grade, exosomal miR-146a-5p levels, and angiogenic levels in BCa patients, we hypothesized that miR-146a-5p could affect tumour angiogenesis. For that, an orthotopic mouse model was used. UMUC3-luc cells (5×10^6) with and without overexpression of miR-146a (miR-146a o/e and empty vector, respectively) (Figure 3a) were inserted through a urethra catheter into the bladder (Figure S2a). After 3 weeks, the tumour size of UMUC3-luc miR-146a o/e cells was significantly larger than that of UMUC3-luc empty vector cells ($P < 0.01$), as measured by IVIS imaging (Figure 3b, c).

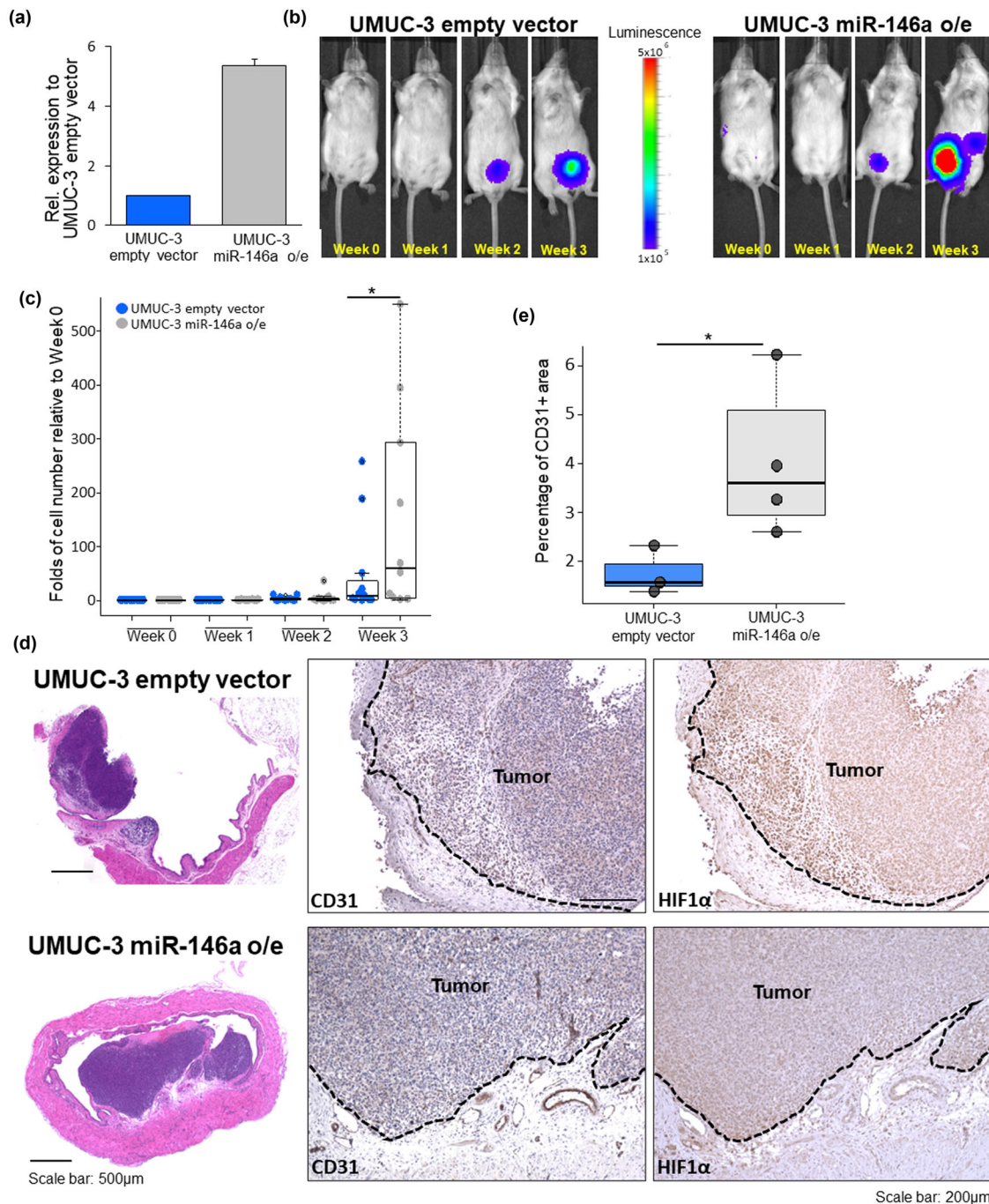


FIGURE 3 miR-146a-5p-overexpressing cells generated tumours highly vascularized. (a) Relative miR-146a-5p expression in UMUC-3-overexpressing cells. (b) Representative bioluminescent images of tumours in C.B.17/SCID mice. (c) Cell growth relative to week 0. (d) Immunohistochemical comparative analysis of UMUC-3 empty vector and UMUC-3 miR-146a o/e. Left: Haematoxylin and eosin staining shows larger tumours in UMUC-3 miR-146a o/e. Center: CD31 staining representing blood vessels. Right: HIF1 α staining represents hypoxic regions. (e) Percentage of CD31+ area in the peritumoural region

Importantly, the size difference was not due to a change in cell proliferation, since *in vitro*, the proliferation was not altered in miR-146a o/e (Figure S2b). Animals were sacrificed, and tumours were resected and stained with the endothelial marker CD31 antibody. Positive CD31 areas, indicating blood vessel area, were more extensive in bladders with tumours composed of UMUC3-luc miR-146a o/e cells (Figure 3d, e). Interestingly, most blood vessels were found in the tumour periphery, in the inner side of the bladder, wrapping the tumour (Figure 3d; Figure S3). To confirm the lack of oxygen due to the low density of vessels, samples were also stained with the hypoxia marker HIF1 α antibody. In accordance, tumours with lower levels of CD31+ area presented higher levels of HIF1 α -stained cells (Figure 3d, right). In summary, miR-146a-5p was observed to promote tumour growth by inducing angiogenesis in an orthotopic mouse model.

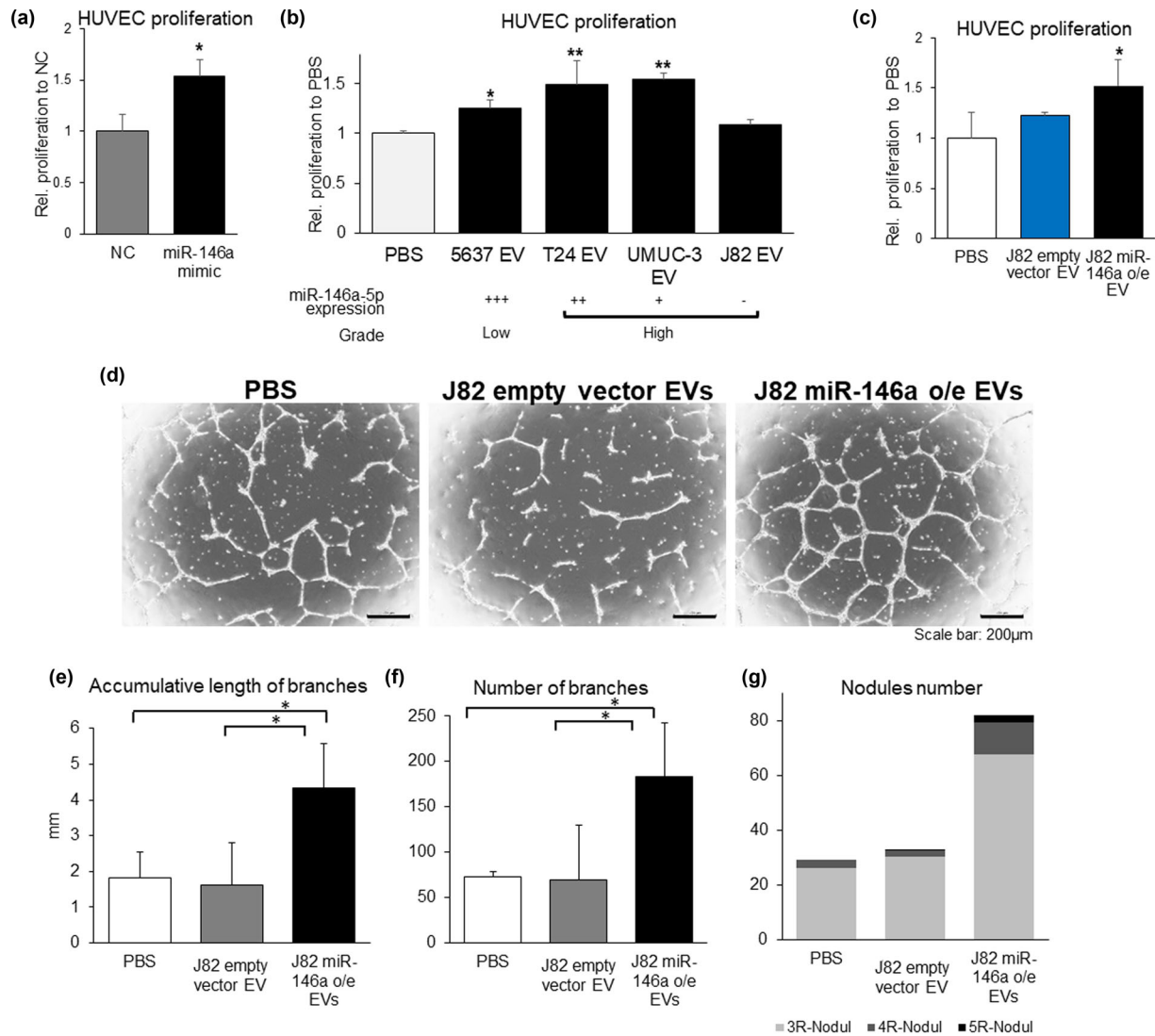


FIGURE 4 High-grade BCa-derived EVs promoted angiogenesis *in vitro*. (a) Relative HUVEC proliferation after miR-146a mimic and nc treatment. (b) Relative cell proliferation of HUVECs under treatment with several BCa-derived EVs. (c) Relative cell proliferation of HUVECs treated with EVs derived from J82 empty vector cells and J82 cells overexpressing miR-146a. (d) Representative image of capillary tube formation in endothelial cells seeded onto Matrigel and treated with EVs. Scale bar: 200 μm. (e) Quantification of the accumulative length of branches in capillary tube formation (in mm). (f) Quantification of the average number of branches. (g) Quantification of ramification per nodule in capillary tube formation

3.3 | miR-146a-5p enriched in EVs from high-grade BCa cells promoted angiogenesis *in vitro*

To confirm the relationship between miR-146a and angiogenesis *in vitro*, human umbilical vascular endothelial cell (HUVEC) proliferation was analysed. Both the addition of miR-146a mimic (Figure 4a) and BCa-derived EVs containing miR-146a-5p induced HUVEC proliferation (Figure 4b).

While the proliferation of HUVECs was in accordance with the secreted levels of miR-146a-5p in most cell lines, this was not applied to the treatment with the BCa low-grade cell line 5637-EV (Figure 2). Although 5637-EV presented the highest miR-146a-5p expression, its cell proliferation induction effects were lower than those of other cell line-derived EVs (Figure 4b). Within the high-grade BCa cell lines, and in accordance with miR-146a-5p expression, the lowest increase in the proliferation rate was observed in the J82 cell line. However, HUVEC proliferation was significantly increased when stable overexpression of miR-146a in J82 cells (J82 miR-146a o/e) was established (Figure S1d, Figure S4), and their secreted EVs were added to HUVECs in comparison to the negative control (J82 empty vector) EVs ($P = 0.049$) (Figure 4c). The same established cell line, J82 miR-146a o/e, promoted capillary tube formation on Matrigel (Figure 4d), as shown by the increase in the length and the number of branches, as well as the number of nodules, especially nodules containing four and five ramifications (Figure 4e-g).

To corroborate that the effect on HUVECs was due to the EV content, the internalization of EVs derived from several cell lines by HUVECs was analysed by immunofluorescence staining. Although all the different cell lines internalized EVs, the uptake

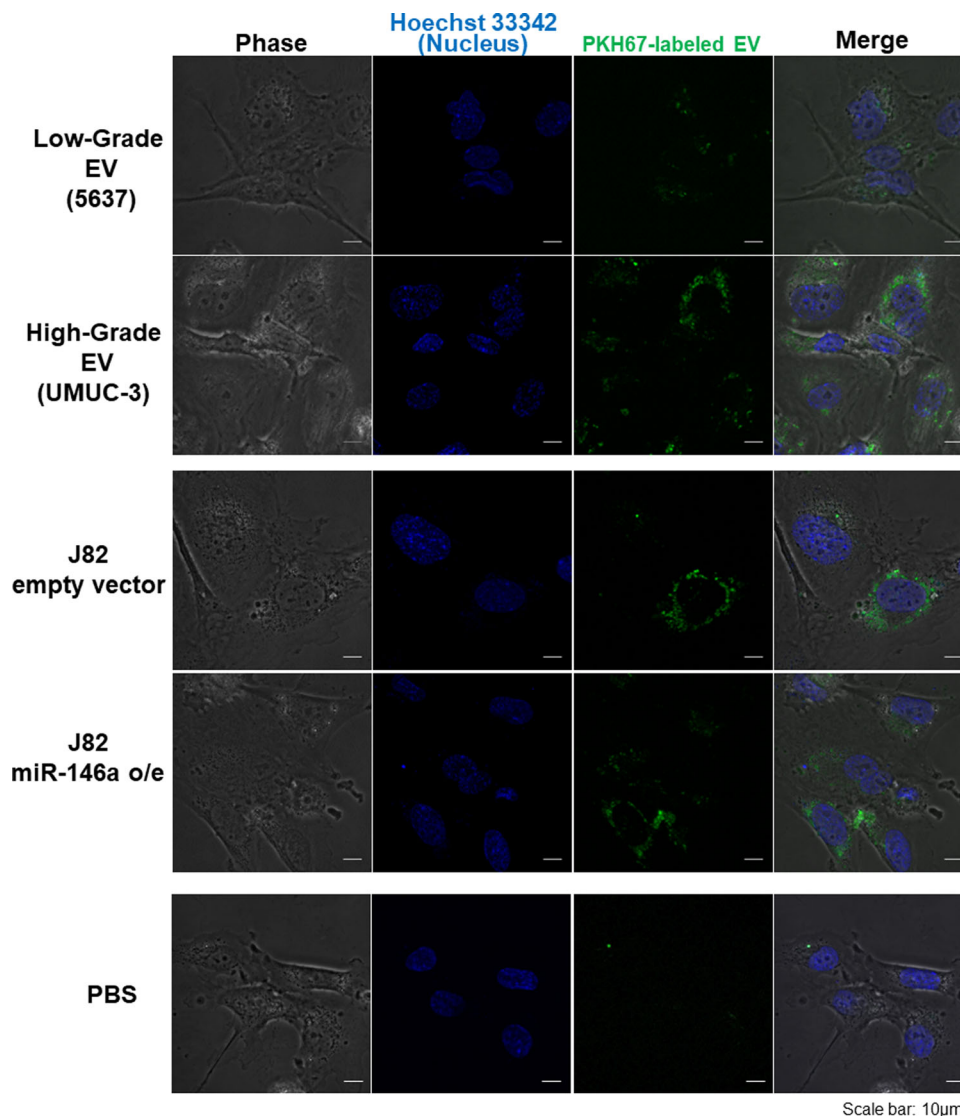


FIGURE 5 High-grade BCa EVs are more effectively internalized. Representative image of EV internalization. EVs stained with PKH67 were added to HUVECs and cultured for 12 h before taking the pictures. PBS was used as a negative control. Scale bar: 10 μ m

efficiency was different (Figure 5). The low-grade cell line 5637 showed the lowest internalization by HUVECs (Figure 5). This result supports the previous observation, in which those cells only slightly promoted HUVEC proliferation (Figure 4b) despite being the cell line with the highest miR-146a-5p expression levels (Figure 2a,b). On the other hand, J82 empty vector and J82 miR-146a o/e were similarly taken up and similar to the UMUC-3 cell line, the other high-grade cell line (Figure 5). These results indicated that HUVECs internalized BCa-derived EVs more effectively from high-grade BCa and that cell proliferation induction was promoted by miR-146a-5p (Figure 4b).

3.4 | TET2 and its downstream target c-Myc are the targets of miR-146a-5p

To identify the target gene of miR-146a-5p in HUVECs, we performed a microarray of HUVECs after several EV treatments. The groups were divided into high levels of miR-146a-5p (5637 EV, T24 EV, UMUC-3 EV, J82 miR-146a o/e EV) and low levels of miR-146a-5p (PBS, J82 empty vector EV) (Figure 6a, Figure S5A). As a result, 557 genes were selected as candidates for the miR-146a-5p target. Next, we compared the paired samples 5637 EV, T24 EV, UMUC-3 EV *versus* PBS; J82 miR-146a o/e EV *versus* J82 empty vector EV; and miR-146a mimic and mimic NC. Genes with a difference of ± 1 -fold change in those comparisons were selected. In total, 22 genes were found (Table S3). Subsequently, to identify the possible target genes from miR-146a-5p, target scan was used, and five genes were selected. Target scan is a bioinformatic tool that identifies microRNA targets by the binding region of the microRNAs (Bartel, 2009). The top five identified target genes by Target scan were ANKRD5, CYB5R4, TET2,

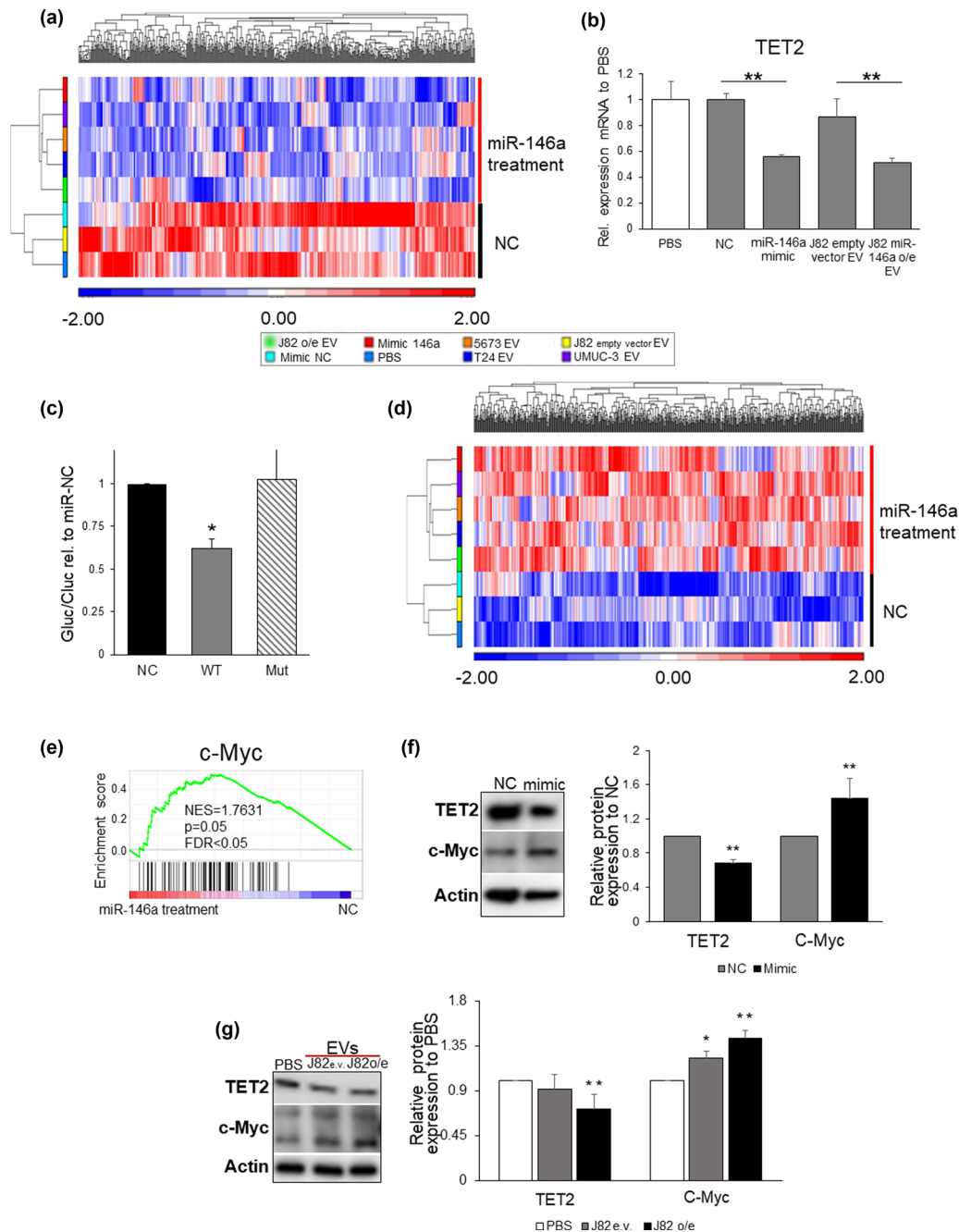


FIGURE 6 TET2 is the target gene of miR146a-5p. (a) Hierarchical clustering analysis of a heatmap indicating the downregulated genes after the treatment of HUVECs with miR-146a in comparison to vector control. The X-axis shows mRNA expression levels of the microarray and the left Y-axis shows the cluster classification of each sample (the red one is miR-146a treatment and the black one is NC). (b) Relative TET2 mRNA expression in HUVECs. Data are represented as the mean of $3 \pm s.d$ replicates. (c) Luciferase activity in HEK 293 cells constructed with the pTK-Gluc reporter construct containing the 3'UTR of TET2, the wild type or containing a mutation. The results indicate that miR-146a directly binds the TET2 3'UTR. (d) A hierarchical clustering analysis of a heatmap of the upregulated genes after the treatment of HUVECs with miR-146a in comparison to vector control. The X-axis shows mRNA expression levels of the microarray and left Y-axis shows cluster classification of each sample (the red one is miR-146a treatment and the black one is NC). C-Myc expression was 1.2-fold higher in miR-146a mimic-treated HUVECs in comparison with the NC group. (e) Enrichment score of c-Myc. (f) Immunoblotting analysis of TET2 and C-Myc expression levels in HUVECs after miR-146a mimic addition ($n = 3$). Left: Representative image of immunoblotting. Right: Average of quantitative values relative to Actin expression ($n = 3$). TET2 PBSversus J82 miR-146a o/e $P = 0.001$; c-Myc PBSversus miR-146a o/e $P = 0.0004$

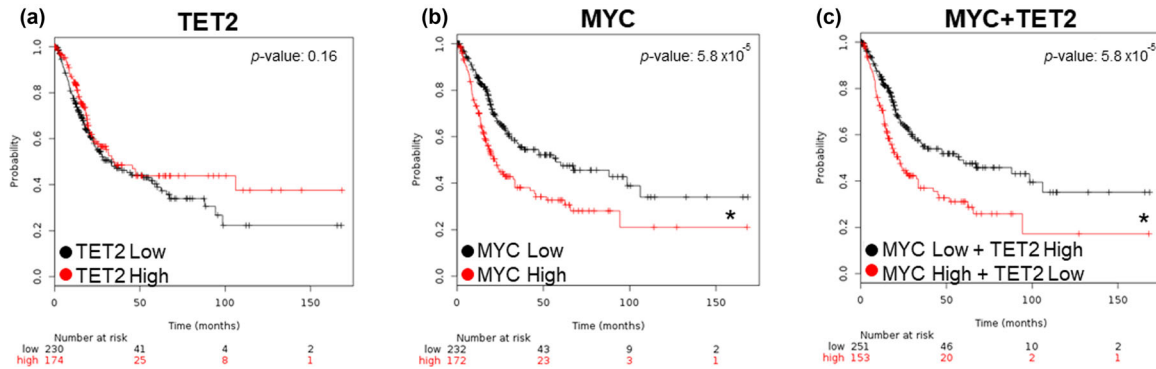


FIGURE 7 Low levels of TET2, along with high levels of MYC, represent a poor prognosis for BCa. Kaplan–Meier representations of the probabilities of overall survival in 404 patients with BCa. The *P* values were calculated using log-rank tests

ZNF667, and ZNF850 (Figure S5a). Their expression was validated by qPCR, and only two out of the previous genes, CY5R4 and TET2, showed lower expression after treatment with miR-146a mimic and J82 miR-146a o/e (Figure 6b and Figure S5b–e). Among these two genes, we focused on TET2 because TET2 is a modulator of DNA demethylation, and its expression has been found to be a tumour suppressor in leukaemia and other blood malignancies (Bensberg et al., 2021; Jiang, 2020); moreover, it has also been related to angiogenesis (Li et al., 2018).

Using the 3-UTR assay, the direct target of miR-146a-5p of TET2 was confirmed (Figure 6c). HEK 293 cells were cotransfected with miR-146a-5p mimic or a negative control mimic and an expression vector containing the luciferase reporter vector harbouring the 3'UTR of TET2 of the wild-type or mutated miR-146a-5p-binding site (Figure 6c). Luciferase activity in cells transfected with miR-146a-5p was reduced in comparison to the negative control miRNA in the wild-type TET2 sequence. In contrast, it was not reduced in the mutated sequence, indicating direct binding.

Subsequently, TET2 downstream was analysed. Using the previous microarray data, we searched for genes whose expression was increased in the presence of miR-146a-5p (Figure S5a; Figure 6d). c-Myc expression in miR-146a mimic-treated HUVECs was upregulated by 1.2-fold in comparison with that in the NC group (Figure 6d), and the enrichment score was 1.76 (Figure 6e). To validate these values, we next analysed protein expression. miR-146a mimic addition to HUVECs decreased TET2 and increased c-Myc protein expression (Figure 6f). Furthermore, the same effect of EVs was confirmed. Only HUVECs treated with EVs derived from J82 miR-146a o/e and empty vector showed a significant decrease in TET2 expression. Significant differences were observed in c-Myc expression by both treatments, but the expression was higher in miR-146a-overexpressing EVs (Figure 6g).

3.5 | TET2 was correlated with the survival rate in bladder cancer by promoting c-Myc

Finally, Kaplan–Meier analysis was performed to study the effect of the identified targets of miR-146a-5p on the overall survival rate in BCa (Figure 7). Low TET2 levels and high c-Myc levels, per se, were correlated with worse BCa prognosis (Figure 7a). However, the difference in overall survival was greater when patients with both low TET2 and high c-Myc expression were sorted together, indicating that the miR-146a-5p target is indeed essential in BCa (Figure 7c).

4 | DISCUSSION

Circulating miRNAs encapsulated in EVs have been proposed as biomarkers for detecting recurrence in BCa. Since urine is a very feasible accessible biofluid, it is arousing much interest (Batista et al., 2020). However, EVs are communication gadgets among cells, and thus, their role in the tumour microenvironment must not be neglected. We previously detected high urinary levels of miR-146a-5p in patients with BCa; however, the function of this miRNA has not yet been elucidated. Here, we describe a novel role of miR-146a-5p in promoting tumour growth and progression by inducing angiogenesis. miR-146a-5p secreted by BCa cells is internalized by ECs, where it directly binds the 3-UTR of TET2, a demethylase responsible for the regulation of c-Myc, among others. Upon EV internalization, TET2 gene expression was reduced, and c-Myc expression increased. c-Myc is an oncogene that promotes cell division, and in ECs, this cell proliferation is transformed into angiogenesis.

High-grade BCa cells secrete EVs that are important modulators of the tumour microenvironment. The importance of intercellular communication has been widely described, and one of these tools are EVs. Cancer cells secrete EVs to both nearby cells and distal sites, transferring a variety of molecules that modify the surroundings, which in turn favours cancer cell growth (He et al., 2015; Peinado et al., 2012; Salomon et al., 2013; Skog et al., 2008). In concrete, we found that

EVs secreted from high-grade BCa induced angiogenesis by promoting EC growth. Angiogenesis is a crucial process for the development of tumours since it supplies cancer cells with oxygen and the nutrients necessary for their growth (Carmeliet, 2000). In accordance, tumours generated by highly expressing miR-146a-5p cells presented less hypoxia. The effect of EVs on tumour angiogenesis is not an unusual concept (Kikuchi et al., 2019). EVs from glioma were found to regulate the VEGF signalling pathway (Ludwig et al., 2018; Sun et al., 2017). In our experiments, we used an overexpression model, in which we observed higher tumour vascularization. In a separate study on colon cancer, inhibition of miR-146a showed a decrease in angiogenesis in a mouse model (Simanovich et al., 2018). Indeed, several other studies support the role of miR-146a in angiogenesis (Simanovich et al., 2018; Zhu et al., 2016). Notably, the outcome of an increased tumour vasculature was also revealed *in vivo* experiments, since those tumours presented a higher tumour growth, possibly due to the fewer restrictions of hypoxia.

The use of EVs as biomarkers in body fluids is currently widespread. Even though EVs carry many molecules, including proteins, lipids, and nucleic acids, they are especially the later ones are auspicious due to the high sensitivity of the detection techniques, such as qPCR. Urinary miRNAs have been reported to correlate with multiple diseases, including BCa, mainly due to their proximity to the urinary tract (Carlos & Slack, 2006; Uchino et al., 2013; Xiu et al., 2014). We have previously reported that miR-146a-5p expression in urine was high in patients with BCa (Sasaki et al., 2016). This miRNA has already been found in relation to various diseases (Chen et al., 2013; Garcia et al., 2011; Wotschofsky et al., 2016), such as in the serum of lung adenocarcinoma (Lv et al., 2017; Wang et al., 2015). In breast cancer, overexpression of miR-146a-5p was also observed to promote cell proliferation of cancer cells by the regulation of the BRCA1 gene (Gao et al., 2018; Garcia et al., 2011). In our study, we did not find an effect on proliferation in BCa cell lines. Instead, we found that miR-146a-5p exerts its effects on EC. Similarly, miR-146a levels were increased in HUVECs after coculture with hepatocellular carcinoma cells (Iacona & Lutz, 2019). The use of miR-146a-5p expression in patients urine as a biomarker for bladder is very promising due to the low invasiveness of the detection and the high recurrent nature of bladder cancer (Sasaki et al., 2016).

miR-146a-5p directly targets TET2 and decreases its expression in EC, increasing c-Myc and eventually translating into angiogenesis activation. TET2 plays an important role in DNA demethylation (Kunimoto & Nakajima, 2021). Indeed, the loss of function of TET2 has been found in haematologic cancers, varying from 10 to 50% depending on the type of neoplasm (Abdel-Wahab et al., 2009; Delhommeau et al., 2009; Jankowska et al., 2009). TET2 has also been related to angiogenesis by the activation of the protein Roundabout4 (Tanaka et al., 2018). In this study, we found that TET2 regulated c-Myc. Under both miR-146a mimic and EV treatment, TET2 was repressed, and c-Myc expression was increased. These results are similar to the paper by Palam LR et al. in myeloid cells (Palam et al., 2018). Although the direct regulation of c-Myc by TET2 was not unravelled in this study, Bensberg *et al.* reported that TET2 regulates c-Myc through PTEN pathway (Bensberg et al., 2021). The c-Myc gene is one of the most favoured oncogenic genes in various malignancies. Moreover, the role of c-Myc in neovascularization is well established by several modes of action (Brandvold et al., 2000; Pelengaris et al., 1999), one of which involves functioning as a master regulator of cytokines, such as VEGF (Kerbel et al., 1998; Pelengaris et al., 1999). Cell proliferation is also essential for the angiogenesis phenomenon, where ECs have to proliferate to enlarge the vasculature. c-Myc induces cell proliferation by entering the DNA synthetic phase of the cell cycle (De Alboran et al., 2001). Hsieh et al. reported that EVs secreted from multiple myeloma cells enriched in miR-146a-5p induced the proliferation of mesenchymal stem cells (Hsieh et al., 2013). In accordance with previous reports, treatment with miR-146a-5p mimic induced cell proliferation in HUVECs. Furthermore, the expression of VEGFA was increased, as found in the microarray data (data not shown).

High-grade BCa cell-derived EVs were more effective at inducing EC proliferation. Low-grade BCa, despite being the cell line with the highest miR-146a-5p expression, did almost not induce HUVEC proliferation. In addition, we did not find differences in EV secretion between high- and low-grade tumours. Interestingly, but we observed differences in uptake efficiency by ECs. Other authors showed that the transfer of EVs from B16 melanoma cells to healthy cells was more common than the internalization of healthy cell-derived EVs by melanoma cells in an *in vivo* system (Zomer et al., 2015). This behaviour is highly likely to be related to the EV membrane since it is known that its composition is important for EV uptake (Mulcahy et al., 2014). Therefore, more malignant cell-derived EVs could present different membrane compositions, as it has been shown that the integrin composition of EVs influences metastatic organotropism (Hoshino et al., 2015). This topic is fascinating and should be addressed in the future.

In conclusion, we found that miR-146a-5p-enriched EVs from high-grade BCa cells promoted angiogenesis and BCa tumour growth by TET2 inhibition and further c-Myc expression activation. Interestingly, the amount of uptaken EVs in HUVECs was significantly different according to the BCa grade. Further studies should address this difference and focus on the EV membrane structure from these cancer cells. Understanding the mechanisms of cancer progression will help us to develop in the future novel therapies.

ACKNOWLEDGEMENTS

We appreciate the contribution of Nobuyoshi Kosaka, Shiari Nozawa and Satoe Aratake for helpful experiments and discussion. The present work was supported in part by a 'Development of Diagnostic Technology for Detection of miRNA in Body Fluids' grant from the Japan Agency for Medical Research and Development (AMED) and a Grant-in-Aid for Young Scientists JSPS KAKENHI Grant Number: 21K16759.

AUTHOR CONTRIBUTIONS

Wataru Usuba, Marta Prieto-Vila and Yusuke Yamamoto carried out the experiments *in vitro* and *in vivo*. Wataru Usuba, Marta Prieto-Vila, Yusuke Yamamoto and YYa analysed the data and prepared the paper draft. Hideo Sasaki and Miki Yoshiike collected and stored urine and FFPE samples. Fumitaka Takeshita, Miki Yoshiike, Hideo Sasaki, Eiji Kikuchi and Takahiro Ochiya conceived the experimental design of the study. All authors read and approved the final manuscript. WU, PV-M and YYo carried out the experiments *in vitro* and *in vivo*. WU, PV-M, YYo and YYa analyzed the data and prepared the paper draft.

CONFLICT OF INTERESTS

The authors declare that they have no competing financial interests.

ORCID

Takahiro Ochiya  <https://orcid.org/0000-0002-0776-9918>

REFERENCES

- Abdel-Wahab, O., Mullally, A., Hedvat, C., Garcia-Manero, G., Patel, J., Wadleigh, M., Malinge, S., Yao, J., Kilpivaara, O., Bhat, R., Huberman, K., Thomas, S., Dolgalev, I., Heguy, A., Paietta, E., Le Beau, M. M., Beran, M., Tallman, M. S., Ebert, B. L., ... Levine, R. L. (2009). Genetic characterization of TET1, TET2, and TET3 alterations in myeloid malignancies. *Blood*, *114*, 144–147.
- Bartel, D. P. (2004). MicroRNAs: Genomics, biogenesis, mechanism, and function. *Cell*, *116*, 281–297.
- Bartel, D. P. (2009). MicroRNAs: Target recognition and regulatory functions. *Cell*, *136*, 215–233.
- Batista, R., Vinagre, N., Meireles, S., Vinagre, J., Prazeres, H., Leão, R., Máximo, V., & Soares, P. (2020). Biomarkers for bladder cancer diagnosis and surveillance: A comprehensive review. *Diagnostics*, *10*, 1–19.
- Bensberg, M., Rundquist, O., Selimovic, A., Lagerwall, C., Benson, M., Gustafsson, M., Vogt, H., Lentini, A., & Nestor, C. E. (2021). TET2 as a tumor suppressor and therapeutic target in T-cell acute lymphoblastic leukemia. *Proceedings of the National Academy of Sciences of the United States of America*, *118*, e2110758118.
- Brandvold, K. A., Neiman, P., & Ruddell, A. (2000). Angiogenesis is an early event in the generation of myc-induced lymphomas. *Oncogene*, *19*, 2780–2785.
- Carlos, S. E., & Slack, F. J. (2006). The role of microRNAs in cancer. *Target Therapy Translational Cancer Research*, *79*, 131–140.
- Carmeliet, P. (2000). Mechanisms of angiogenesis and arteriogenesis. *Nature Medicine*, *6*, 389–395.
- Carthew, R. W., & Sontheimer, E. J. (2009). Origins and mechanisms of miRNAs and siRNAs. *Cell*, *136*, 642–655.
- Chen, G., Umelo, I. A., Lv, S., Teugels, E., Fostier, K., Kronenberger, P., Dewaele, A., Sadones, J., Geers, C., & De Grève, J. (2013). miR-146a inhibits cell growth, cell migration and induces apoptosis in non-small cell lung cancer cells. *Plos One*, *8*, 1–13.
- Damrauer, J. S., Hoadley, K. A., Chism, D. D., Fan, C., Tiganelli, C. J., Wobker, S. E., Yeh, J. J., Milowsky, M. I., Iyer, G., Parker, J. S., & Kim, W. Y. (2014). Intrinsic subtypes of high-grade bladder cancer reflect the hallmarks of breast cancer biology. *Proceedings of the National Academy of Sciences of the United States of America*, *111*, 3110–3115.
- De Alboran, I. M., O'hagan, R. F., Gärtner, F., Malynn, B., Davidson, L., Rickert, R., Rajewsky, K., Depinho, R. A., & Alt, F. W. (2001). Analysis of c-Myc function in normal cells via conditional gene-targeted mutation. *Immunity*, *14*, 45–55.
- Delhommeau, F., Dupont, S., Della Valle, V., James, C., Trannoy, S., Massé, A., Kosmider, O., Le Couedic, J.-P., Robert, F., Alberdi, A., Lécluse, Y., Plo, I., Dreyfus, F. J., Marzac, C., Casadevall, N., Lacombe, C., Romana, S. P., Dessen, P., Soulier, J., ... Bernard, O. A. (2009). Mutation in TET2 in myeloid cancers François. *New England Journal of Medicine*, *360*, 2289–2301.
- Deregibus, M. C., Cantaluppi, V., Calogero, R., Lo Iacono, M., Tetta, C., Biancone, L., Bruno, S., Bussolati, B., & Camussi, G. (2007). Endothelial progenitor cell - Derived microvesicles activate an angiogenic program in endothelial cells by a horizontal transfer of mRNA. *Blood*, *110*, 2440–2448.
- Gao, W., Hua, J., Jia, Z., Ding, J., Han, Z., Dong, Y., Lin, Q., & Yao, Y. (2018). Expression of miR-146a-5p in breast cancer and its role in proliferation of breast cancer cells. *Oncology Letters*, *15*, 9884–9888.
- Garcia, A. I., Buisson, M., Bertrand, P., Rimokh, R., Rouleau, E., Lopez, B. S., Lidereau, R., Mikaélian, I., & Mazoyer, S. (2011). Down-regulation of BRCA1 expression by miR-146a and miR-146b-5p in triple negative sporadic breast cancers. *EMBO Molecular Medicine*, *3*, 279–290.
- Gould, S. J., & Raposo, G. (2013). As we wait: Coping with an imperfect nomenclature for extracellular vesicles. *Journal of Extracellular Vesicles*, *2*, 20389.
- He, M., Qin, H., Poon, T. C. W., Sze, S.-C., Ding, X., Co, N. N., Ngai, S.-M., Chan, T.-F., & Wong, N. (2015). Hepatocellular carcinoma-derived exosomes promote motility of immortalized hepatocyte through transfer of oncogenic proteins and RNAs. *Carcinogenesis*, *36*, 1008–1018.
- Hoshino, A., Costa-Silva, B., Shen, T.-L., Rodrigues, G., Hashimoto, A., Tesic Mark, M., Molina, H., Kohsaka, S., Di Giannatale, A., Ceder, S., Singh, S., Williams, C., Soplod, N., Uryu, K., Pharmed, L., King, T., Bojmar, L., Davies, A. E., Ararso, Y., ... Lyden, D. (2015). Tumour exosome integrins determine organotropic metastasis. *Nature*, *527*, 329–335.
- Hsieh, J. - Y., Huang, T.-S., Cheng, S.-M., Lin, W.-S., Tsai, T.-N., Lee, O. K., & Wang, H.-W. (2013). MiR-146a-5p circuitry uncouples cell proliferation and migration, but not differentiation, in human mesenchymal stem cells. *Nucleic Acids Research*, *41*, 9753–9763.
- Iacona, J. R., & Lutz, C. S. (2019). miR-146a-5p: Expression, regulation, and functions in cancer. *Wiley Interdisciplinary Reviews RNA*, *10*, 1–22.
- Jankowska, A. M., Szpurka, H., Tiu, R. V., Makishima, H., Afable, M., Huh, J., O'keefe, C. L., Ganetzky, R., Mcdevitt, M. A., & Maciejewski, J. P. (2009). Loss of heterozygosity 4q24 and TET2 mutations associated with myelodysplastic/myeloproliferative neoplasms. *Blood*, *113*, 6403–6410.
- Jiang, S. (2020). Tet2 at the interface between cancer and immunity. *Communications Biology*, *3*, 1–6.
- Kerbel, R. S., Vitoria-Petit, A., Okada, F., & Rak, J. (1998). Establishing a link between oncogenes and tumor angiogenesis. *Molecular Medicine*, *4*, 286–295.
- Kikuchi, S., Yoshioka, Y., Prieto-Vila, M., & Ochiya, T. (2019). Involvement of extracellular vesicles in vascular-related functions in cancer progression and metastasis. *International Journal of Molecular Sciences*, *20*, 1–17.
- Kosaka, N., Iguchi, H., Yoshioka, Y., Takeshita, F., Matsuki, Y., & Ochiya, T. (2010). Secretory mechanisms and intercellular transfer of microRNAs in living cells. *Journal of Biological Chemistry*, *285*, 17442–17452.
- Kunimoto, H., & Nakajima, H. (2021). TET2: A cornerstone in normal and malignant hematopoiesis. *Cancer Science*, *112*, 31–40.
- Lánczky, A., & Györfy, B. (2021). Web-based survival analysis tool tailored for medical research (KMplot): Development and implementation. *Journal of Medical Internet Research [Electronic Resource]*, *23*, 1–7.
- Lenis, A. T., Lec, P. M., Chamie, K., & Mshs, M. (2020). Bladder cancer a review. *JAMA - Journal of the American Medical Association*, *324*, 1980–1991.

- Li, X., Wu, C., Shen, Y., Wang, K., Tang, L., Zhou, M., Yang, M., Pan, T., Liu, X., & Xu, W. (2018). Ten-eleven translocation 2 demethylates the MMP9 promoter, and its down-regulation in preeclampsia impairs trophoblast migration and invasion. *Journal of Biological Chemistry*, 293, 10059–10070.
- Ludwig, N., Yerneni, S. S., Razzo, B. M., & Whiteside, T. L. (2018). Exosomes from HNSCC promote angiogenesis through reprogramming of endothelial cells. *Molecular Cancer Research*, 16, 1798–1808.
- Lv, S., Xue, J., Wu, C., Wang, L., Wu, J., Xu, S., Liang, X., & Lou, J. (2017). Identification of a panel of serum microRNAs as biomarkers for early detection of lung adenocarcinoma. *Journal of Cancer*, 8, 48–56.
- Mulcahy, L. A., Pink, R. C., & Carter, D. R. F. (2014). Routes and mechanisms of extracellular vesicle uptake. *Journal of Extracellular Vesicles*, 3, 1–14.
- Nishida, N., Yano, H., Nishida, T., Kamura, T., & Kojiro, M. (2006). Angiogenesis in cancer. *Vascular Health and Risk Management*, 2, 213–219.
- Oude Elferink, P., & Witjes, J. A. (2014). Blue-light cystoscopy in the evaluation of non-muscle-invasive bladder cancer. *Therapeutic Advances in Urology*, 6, 25–33.
- Palam, L. R., Mali, R. S., Ramdas, B., Srivatsan, S. N., Visconte, V., Tiu, R. V., Vanhaesebroeck, B., Roers, A., Gerbault, A., Xu, M., Janga, S. C., Takemoto, C. M., Paczesny, S., & Kapur, R. (2018). Loss of epigenetic regulator TET2 and oncogenic KIT regulate myeloid cell transformation via PI3K pathway. *JCI Insight*, 3, 1–20.
- Peinado, H., Alečković, M., Lavotshkin, S., Matei, I., Costa-Silva, B., Moreno-Bueno, G., Hergueta-Redondo, M., Williams, C., Garcá-A-Santos, G., Ghajar, C. M., Nitoro-Hoshino, A., Hoffman, C., Badal, K., Garcia, B. A., Callahan, M. K., Yuan, J., Martins, V. R., Skog, J., Kaplan, R. N., ... Lyden, D. (2012). Melanoma exosomes educate bone marrow progenitor cells toward a pro-metastatic phenotype through MET. *Nature Medicine*, 18, 883–891.
- Pelengaris, S., Littlewood, T., Khan, M., Elia, G., & Evan, G. (1999). Reversible activation of c-Myc in skin: Induction of a complex neoplastic phenotype by a single oncogenic lesion. *Molecular Cell*, 3, 565–577.
- Sadi, M. V. (2017). PSA screening for prostate cancer. *Revista Da Associação Médica Brasileira*, 63, 722–725.
- Salomon, C., Ryan, J., Sobrevia, L., Kobayashi, M., Ashman, K., Mitchell, M., & Rice, G. E. (2013). Exosomal signaling during hypoxia mediates microvascular endothelial cell migration and vasculogenesis. *Plos One*, 8, 1–24.
- Sasaki, H., Yoshiike, M., Nozawa, S., Usuba, W., Katsuoka, Y., Aida, K., Kitajima, K., Kudo, H., Hoshikawa, M., Yoshioka, Y., Kosaka, N., Ochiya, T., & Chikaraishi, T. (2016). Expression level of urinary MicroRNA-146a-5p is increased in patients with bladder cancer and decreased in those after transurethral resection. *Clin Genitourin Cancer*, 14, e493–e499.
- Simanovich, E., Brod, V., Rahat, M. M., & Rahat, M. A. (2018). Function of miR-146a-5p in tumor cells as a regulatory switch between cell death and angiogenesis: Macrophage therapy revisited. *Frontiers in Immunology*, 8, 1931.
- Skog, J., Würdinger, T., Van Rijn, S., Meijer, D. H., Gainche, L., Curry, W. T., Carter, B. S., Krichevsky, A. M., & Breakefield, X. O. (2008). Glioblastoma microvesicles transport RNA and protein that promote tumor growth and provide diagnostic biomarkers. *Nature Cell Biology*, 10, 1470–1476.
- Stănescu, F., Geavlete, B., Georgescu, D., Jecu, M., Moldoveanu, C., Adou, L., Bulai, C., Ene, C., & Geavlete, P. (2014). NBI - plasma vaporization hybrid approach in bladder cancer endoscopic management. *Journal of Medicine and Life*, 7, 155–159.
- Sun, X., Ma, X., Wang, J., Zhao, Y., Wang, Y., Bihl, J. C., Chen, Y., & Jiang, C. (2017). Glioma stem cells-derived exosomes promote the angiogenic ability of endothelial cells through miR-21/VEGF signal. *Oncotarget*, 8, 36137–36148.
- Sung, H., Ferlay, J., Siegel, R. L., Laversanne, M., Soerjomataram, I., Jemal, A., & Bray, F. (2021). Global Cancer Statistics 2020: GLOBOCAN estimates of incidence and mortality worldwide for 36 cancers in 185 countries. *CA: A Cancer Journal for Clinicians*, 71, 209–249.
- Tanaka, T., Izawa, K., Maniwa, Y., Okamura, M., Okada, A., Yamaguchi, T., Shirakura, K., Maekawa, N., Matsui, H., Ishimoto, K., Hino, N., Nakagawa, O., Aird, W. C., Mizuguchi, H., Kawabata, K., Doi, T., & Okada, Y. (2018). ETV2-TET1/TET2 complexes induce endothelial cell-specific Robo4 expression via promoter demethylation. *Science Reports*, 8, 1–10.
- Uchino, K., Takeshita, F., Takahashi, R.-U., Kosaka, N., Fujiwara, K., Naruoka, H., Sonoke, S., Yano, J., Sasaki, H., Nozawa, S., Yoshiike, M., Kitajima, K., Chikaraishi, T., & Ochiya, T. (2013). Therapeutic effects of microRNA-582-5p and -3p on the inhibition of bladder cancer progression. *Molecular Therapy*, 21, 610–619.
- Ulmert, D., Serio, A. M., O'Brien, M. F., Becker, C., Eastham, J. A., Scardino, P. T., Björk, T., Berglund, G., Vickers, A. J., & Lilja, H. (2008). Long-term prediction of prostate cancer: Prostate-specific antigen (PSA) velocity is predictive but does not improve the predictive accuracy of a single PSA measurement 15 years or more before cancer diagnosis in a large, representative, unscreened popula. *Journal of Clinical Oncology*, 26, 835–841.
- Wang, R. J., Zheng, Y. H., Wang, P., & Zhang, J. Z. (2015). Serum miR-125a-5p, miR-145 and miR-146a as diagnostic biomarkers in non-small cell lung cancer. *International Journal of Clinical and Experimental Pathology*, 8, 765–771.
- Wotschofsky, Z., Gummlich, L., Liep, J., Stephan, C., Kilic, E., Jung, K., Billaud, J.-N., & Meyer, H.-A. (2016). Integrated microRNA and mRNA signature associated with the transition from the locally confined to the metastasized clear cell renal cell carcinoma exemplified by miR-146-5p. *Plos One*, 11, 1–20.
- Xiu, Y., Liu, Z., Xia, S., Jin, C., Yin, H., Zhao, W., & Wu, Q. (2014). MicroRNA-137 upregulation increases bladder cancer cell proliferation and invasion by targeting PAQR3. *Plos One*, 9, 1–7.
- Yokoi, A., Yoshioka, Y., Yamamoto, Y., Ishikawa, M., Ikeda, S.-I., Kato, T., Kiyono, T., Takeshita, F., Kajiyama, H., Kikkawa, F., & Ochiya, T. (2017). Malignant extracellular vesicles carrying MMP1 mRNA facilitate peritoneal dissemination in ovarian cancer. *Nature Communication*, 8, 14470.
- Zhang, B., Pan, X., Cobb, G. P., & Anderson, T. A. (2007). A microRNAs as oncogenes and tumor suppressors. *Developmental Biology*, 302, 1–12.
- Zhu, H. Y., Bai, W. D., Liu, J. Q., Zheng, Z., Guan, H., Zhou, Q., Su, L. L., Xie, S. T., Wang, Y. C., Li, J., Li, N., Zhang, Y. J., Wang, H. T., & Hu, D. H. (2016). Up-regulation of FGF1 signaling contributes to MIR-146a-induced angiogenesis in human umbilical vein endothelial cells. *Science Reports*, 6, 1–11.
- Zomer, A., Maynard, C., Verweij, F. J., Kamermans, A., Schäfer, R., Beerling, E., Schiffelers, R. M., De Wit, E., Berenguer, J., Ellenbroek, S. I. J., Wurdinger, T., Pegtel, D. M., & Van Rheenen, J. (2015). In vivo imaging reveals extracellular vesicle-mediated phenocopying of metastatic behavior. *Cell*, 161, 1046–1057.

SUPPORTING INFORMATION

Additional supporting information can be found online in the Supporting Information section at the end of this article.

How to cite this article: Prieto-Vila, M., Usuba, W., Yoshioka, Y., Takeshita, F., Yoshiike, M., Sasaki, H., Yamamoto, Y., Kikuchi, E., & Ochiya, T. (2022). High-grade bladder cancer cells secrete extracellular vesicles containing miRNA-146a-5p and promotes angiogenesis. *Journal of Extracellular Biology*, 1, e47. <https://doi.org/10.1002/jex2.47>